The X-ray halo of GX5-1

Randall K. Smith

Code 662, NASA/Goddard Space Flight Center, Greenbelt, MD 20771
Department of Physics and Astronomy, The Johns Hopkins University, Baltimore, MD 21218, USA

rsmith@milkyway.gsfc.nasa.gov

T. M. Dame

Harvard-Smithsonian Center for Astrophysics, 60 Garden St., Cambridge, MA 02138, USA

Elisa Costantini

SRON National Institute for Space Research, Sorbonnelaan, 2, 3584CA, Utrecht, The Netherlands
Astronomical Institute, Utrect University, P.O. Box 80000, 3508TA Utrecht, The Netherlands

Peter Predehl

Max-Planck-Institut für extraterrestrische Physik, Giessenbachstr. 1, D-85748 Garching bei München, Germany

ABSTRACT

Using *Chandra* observations we have measured the energy-resolved dust-scattered X-ray halo around the low-mass X-ray binary GX5-1, detecting for the first time multiply scattered X-rays from interstellar dust. We compared the observed X-ray halo at various energies to predictions from a range of dust models. These fits used both smoothly-distributed dust as well as dust in clumped clouds, with CO and 21 cm observations helping to determine the position of the clouds along the line of sight. We found that the BARE-GR-B model of Zubko, Dwek & Arendt (2004) generally led to the best results, although inadequacies in both the overall model and the data limit our conclusions. We did find that the composite dust models of Zubko, Dwek & Arendt (2004), especially the "no carbon" models, gave uniformly poor results. Although models using cloud positions and densities derived naively from CO and 21 cm data gave generally poor results, plausible adjustments to the distance of the largest cloud and the mass of a cloud in the expanding 3 kpc Arm lead to significantly improved fits. We suggest that combining X-ray halo, CO, and 21 cm observations will be a fruitful method to improve our understanding of both the gas and dust phases of the interstellar medium.

Subject headings: dust — scattering — X-rays: binaries — X-rays: ISM

1. Introduction

Although interstellar (IS) dust is a significant component of dense molecular clouds, measuring the properties of these grains is difficult. Except in the outskirts of the clouds, the inherently large extinction prevents optical and UV measurements except in unusual circumstances. As a result, information about the size distribution and composition of grains in dense clouds has by necessity been extrapolated from

observations of less-dense clouds or modeled based on IR measurements. We show that X-ray scattering observations, combined with CO spectral line measurements, can put useful limits on the allowed dust models.

Our X-ray source is the low-mass X-ray binary (LMXB) GX5-1. GX5-1 is a Z source (see van der Klis 1995, and references therein), and is the second brightest persistent Galactic X-ray source after the Crab Nebula. The secondary has been imaged in the IR (Jonker et al. 2000) but the IR spectra measured by Bandyopadhyay et al. (2003) could not be typed. Christian & Swank (1997) estimated the distance to be 9 kpc, although they warned that this is probably an upper limit to the distance and assigned an error of 2.7 kpc to the value. Using X-ray spectra taken by the *Einstein* satellite they also measured the column density to be $N_{\rm H} = 2.54 \pm 0.19 \times 10^{22}\,{\rm cm}^{-2}$, although this result depends on the assumed spectral model. Recently, Ueda et al. (2005) used a *Chandra* HETG observation to measure the depth of absorption edges of a number of IS metals along the line of sight to GX5-1. Based on these measurements, they determined the total $N_{\rm H} = 2.8^{+3.3}_{-1.8} \times 10^{22}\,{\rm cm}^{-2}$; this result has larger error bars than the Christian & Swank (1997) value, primarily because it does not assume a spectral model *a priori*.

The X-ray halo around GX5-1 has been observed by many X-ray satellites, albeit with lower angular or energy resolution than is possible with the *Chandra* ACIS. Predehl et al. (1992) used a lunar occultation of GX5-1 to measure the scattered halo directly, finding a total halo intensity (in the ROSAT band) 28% of the source intensity. GX5-1 was also included in the Predehl & Schmitt (1995) survey of X-ray halos detected with ROSAT, where they measured a halo intensity 25.4% of the source intensity. Recently, Xiang, Zhang, & Yao (2005) analyzed 17 X-ray sources, including GX5-1, using a new technique based on the zero-order image of *Chandra* HETG data. They found a lower total halo intensity (9.9%), as expected since the *Chandra* bandpass extends to higher energies where halo intensities are smaller. They also measured a total column density $N_{\rm H} = 2.0 \times 10^{22}\,{\rm cm}^{-2}$ and fit their data to determine the relative dust positions along the line of sight, finding that 90% of the dust was within 10% of the source.

2. Theoretical Framework

Overbeck (1965) first described astrophysical X-ray halos, which result from small-angle scattering of X-rays inside solid matter. The technique has long been used in laboratory studies of virii or proteins in solution, as careful measurements of the radial profile can show the density and shape of the particles (Guinier & Fournet 1955). The theory of X-ray halos in an astrophysical setting has been described in detail by a number of authors (Mauche & Gorenstein 1986; Mathis & Lee 1991; Smith & Dwek 1998; Draine 2003). We briefly review the theory here.

The fundamental quantity is the differential scattering cross section $d\sigma/d\Omega$, which can be calculated using either the exact Mie solution or the Rayleigh-Gans (RG) approximation; see Smith & Dwek (1998) for a discussion. As the RG approximation is analytic it demonstrates how the various parameters scale:

$$\frac{d\sigma(\theta_{\rm sca})}{d\Omega} = 1.1\,{\rm cm}^2{\rm sr}^{-1}\left(\frac{2Z}{M}\right)^2\left(\frac{\rho}{3{\rm g\,cm}^{-3}}\right)^2 a_{\mu{\rm m}}^6\left(\frac{F(E)}{Z}\right)^2\Phi^2(\theta_{\rm sca}) \qquad (1)$$

where a is the grain radius, Z the mean atomic charge, M the mean atomic weight (in amu), ρ the mass density, E the X-ray energy in keV, $F(E)$ the atomic scattering factor (Henke 1981), $\theta_{\rm sca}$ the scattering angle, and $\Phi^2(\theta_{\rm sca})$ the scattering form factor (Mathis & Lee 1991). For homogeneous spherical grains, the form factor is given by $\Phi^2(\theta_{\rm sca}) = 3(\sin u - u\cos u)/u^3$ where $u = 4\pi a \sin(\theta_{\rm sca}/2)/\lambda \approx 2\pi a\theta_{\rm sca}E/hc$.

Smith & Dwek (1998) showed that the RG approximation will overestimate the total scattering if the energy of the X-rays (in keV) is not substantially larger than the size of the dust grains (in μm), and suggested 2 keV as a minimum energy for most ISM dust models.

By integrating the scattering cross section over the line of sight geometry, the source spectrum, and the dust size distribution we get (considering single scatterings only) the halo surface brightness at angle θ from the source:

$$I_{\rm sca}(\theta) = F_X N_H \int dE\, S(E) \int da\, n(a) \int_0^1 dx\, \frac{f(x)}{(1-x)^2} \frac{d\sigma}{d\Omega} \tag{2}$$

where F_X is the total source flux, $N_{\rm H}$ is the hydrogen column density, $S(E)$ is the (normalized) X-ray spectrum, and $n(a)da$ is the dust grain size distribution. Here $f(x)$ is the density of hydrogen at distance xD from the observer divided by the line of sight average density, where D is the distance to the source (Mathis & Lee 1991).

2.1. Multiple Scattering

If the column density is sufficiently large, individual X-rays may be scattered multiple times. Mathis & Lee (1991) showed that for $\tau_{\rm sca} > 1.3$, there are more multiply scattered photons than singly scattered. Multiple scatting tends to broaden the halo in an energy-dependent fashion. The scattering cross section itself depends upon the X-ray energy and the dust model; Table 1 of Mathis & Lee (1991) shows that $\sigma_{\rm sca} = 9.03 \times 10^{-23} E_{\rm keV}^{-2}$ for dust models such as Mathis, Rumpl & Nordsieck (1977, MRN77) or Draine & Lee (1984). For $N_{\rm H} \approx 4 \times 10^{22}\,{\rm cm}^{-2}$ (see §3.4), this corresponds to $\tau_{\rm sca} = 3.6 E_{\rm keV}^{-2}$. Below 2 keV, we therefore expect both that the RG approximation will overestimate the total halo intensity and that the single scattering approximation will underestimate the radial extent of the halo. At 2 keV, however, the RG approximation is adequate and although multiple scattering does not dominate, it will still observably broaden the halo. By 3 keV, however, single scattering entirely dominates.

Explicitly calculating all possible scatterings is difficult, but it is possible to calculate the radial profile including both single and double scattering. Both Mathis & Lee (1991) and Predehl & Klose (1996) derived the general form for the total cross section including multiple dust scattering. Using the Gaussian approximation to $d\sigma/d\Omega$ derived in ML91, the singly-scattered profile is

$$I^{(1)}(\theta, E) = N_H c_1 (\frac{\rho}{3})^2 \int_{x_0}^{x_1} \frac{dx}{(1-x)^2} \int_{a_0}^{a_1} da n(a) a^6 \exp\left[-0.4575 E^2 a^2 \frac{\theta^2}{(1-x)^2} \right] \tag{3}$$

where $c_1 = 1.1\,{\rm cm}^2{\rm sr}^{-1}$, ρ is the grain density, in g cm^{-3}, a the grain size in μm, $n(a)$ is the dust grain size distribution, and E the X-ray energy in keV.

This can be extended using the recursion relation given in Predehl & Klose (1996) to doubly scattered photons. This result holds for smoothly distributed dust between the x_0 and x_1. In the following, we take advantage of the small-angle nature of the scattering to simplify some of the trigonometry. As a result, the scattering over θ' does not include all possible values of θ' but is limited to $\theta_1 \approx 20'$. With that restriction, the profile for doubly-scattered photons is:

$$\begin{aligned} I^{(2)}(\theta, E) \;=\; & N_H^2 c_1^2 (\frac{\rho}{3})^4 \int_{x_0}^{x_1} dx \int_x^{x_1} \frac{dx'}{(1-x')^2} \int_0^{\theta_1} d\theta' \theta' \int_0^{2\pi} d\phi \times \\ & \int_{a_0}^{a_1} da a^6 n(a) \exp\left[-0.4575 E^2 a^2 (\theta'^2 + \frac{2\theta\theta'}{1-x} \sin\phi) + (\frac{\theta}{1-x})^2 \right] \times \end{aligned} \tag{4}$$

$$\int_{a_0}^{a_1} da' a'^6 n(a') \exp[-0.4575 E^2 a'^2 (\theta' \frac{1-x}{1-x'})^2] \exp[-N_H (x'-x) \sigma_{sca}]$$

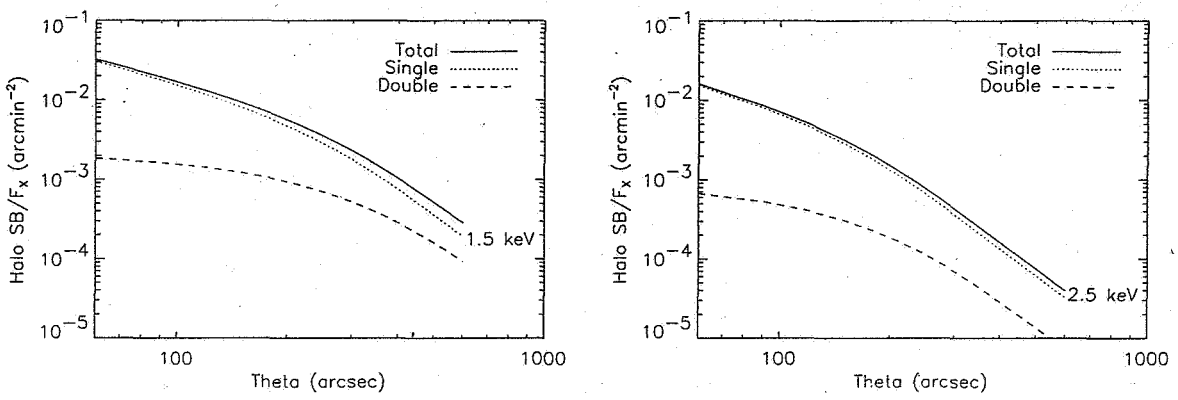

Fig. 1.— Singly- and doubly-scattered surface brightness profiles through a column density of $N_H = 4 \times 10^{22}\,cm^{-2}$ for 1.5 keV [Left] and 2.5 keV [Right] X-rays, through a smoothly distributed MRN77 dust distribution from the observer to 90% of the distance to the source.

To our knowledge, this has no analytic solution. However, it can be solved numerically if $x_1 \neq 1$ (otherwise the solution becomes numerically unstable). We considered smoothly distributed dust between the observer ($x_0 = 0$) and 90% of the distance to the source ($x_1 = 0.9$). The scale of the effect can be seen in Figure 1, which shows the single and double-scattering profiles for $N_H = 4 \times 10^{22}\,cm^{-2}$ at 1.5 and 2.5 keV, assuming an MRN77 dust model. The total power in the doubly-scattered photons is not insignificant. The column density will produce an overall optical depth for scattering $\tau = 1.25$ at 1.5 keV and 0.42 at 2.5 keV. At 1.5 keV, $\sim 50\%$ of the scattered photons will be multiply scattered, and at 2.5 keV, $\sim 20\%$ (Mathis & Lee 1991). However, the effect it has on the profile is significant only at large radii and lower energies. At 2.5 keV, even at large radii, the broadening effect is relatively weak. Due to the twin difficulties of calculating the double scattering and the Mie cross sections we will focus on energies $\gtrsim 2.5\,keV$

3. Data Reduction

GX5-1 was observed by the *Chandra* ACIS-S for 7 ksec on August 6, 2000 (ObsID 109) and $\sim$ 1.5 million counts were detected. Due to the design of the *Chandra* ACIS detector, event "pileup" is a problem for bright sources (Davis 2001). For GX5-1, the pileup is so severe that no counts were detected within a 2.5" radius circle centered at 18:01:08.217, -25:04:41.34 (J2000), after correcting the aspect solution following the Chandra website [1]. We used a similar procedure to that described in Smith, Edgar & Shafer (2002, SES02) to determine the source position for this observation, and estimate the error in this procedure to be $\sim$0.3", in addition to the 0.6" (90% confidence) error in the Chandra aspect reconstruction. Our result is 1.24" from the position determined for the IR counterpart (18:01:08.222, -25:04:42.58, J2000) by Jonker et al. (2000) and 0.7" from the ATCA position (18:01:08.233, -25:04:42.044, J2000) measured by Berendsen et al. (2000).

[1] http://cxc.harvard.edu/cal/ASPECT/fix_offset/fix_offset.cgi

3.1. Pileup

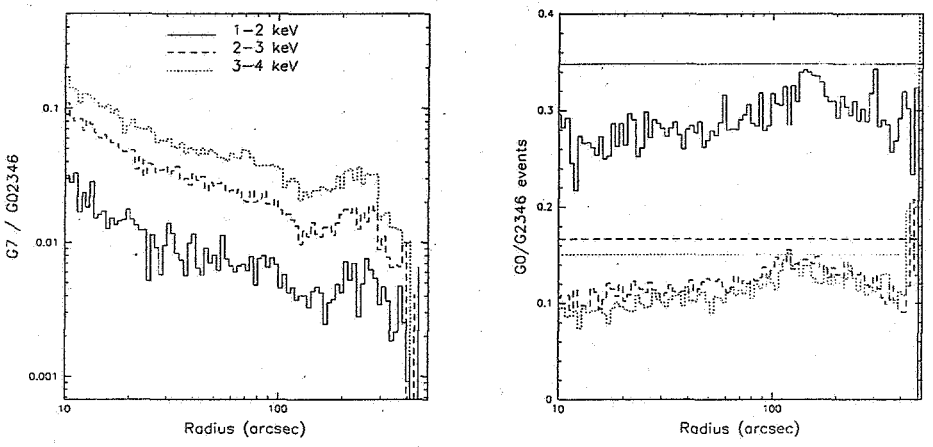

Fig. 2.— (a) Observed radial profile of the ratio of grade 7 events to grade 02346 events on ACIS-S3, in three bands: 1-2 keV, 2-3 keV, and 3-4 keV. Near the source, pileup reduces the number of legal G02346 events as multiple photons are treated as a single multi-pixel event. (b) Same, for grade 0 to grade 2346. For comparison purposes the average ratio measured in Cas A is shown as a flat line.

We now have to measure the radial extent of the pileup, to determine where we can begin to extract radial profiles with confidence. One way to measure this effect is to examine the ratio of 'unphysical' grade 7 (which have detected charge in five or more pixels out of a 3x3 region) to the normally allowed grades 0,2,3,4 and 6 (which have charge in only one to four pixels) as a function of energy and angular distance from the source. As the pileup diminishes, the ratio should approach a constant value if the counts are still dominated by the source, and then transition to the 'background' value far from the source, as shown in Figure 2(a) for three energy bands. In Figure 2(b) we show the ratio of grade 0 (single-pixel events) to grades 2,3,4, and 6 for the same three energy bands. In both cases, the ratios seem to indicate that within 100" of the source, pileup is affecting the grade ratios. Beyond $\sim 250''$ the ratio might change, possibly due to the increasing fraction of background photons. We limited our analysis to radii beyond 100" to avoid possible contamination.

3.2. Spectrum

Measuring the spectrum of a strongly piled-up source is difficult, since the source counts cannot be directly extracted. The so-called "transfer streak," created by mispositioned counts that arrived during the frame transfer provide the only clean unpiled spectrum in the data. The transfer streak has not yet been explicitly calibrated by the Chandra X-ray Center team. Nonetheless an accurate spectral measurement is crucial when subtracting the instrumental PSF as well as calculating the total dust column density. Our approach is similar to that described in SES02, except for the treatment of the background. The source counts were extracted from a 8 pixel wide by 611 pixel long box that stretched across the CCD, with the exception of the region within 100" of GX5-1 (203 pixels), which was excluded to avoid pileup. The allowed region contained 48465 counts, with a total observing time of 6868.7 seconds, or a total of 2146 3.2 second

CCD "frames." Each CCD frame, therefore, had ~ 22.5 counts in the transfer streak, spread over a 8×611 pixel box so pileup in the readout streak is not significant. Since the 8 pixel wide box contains essentially all of the transfer streak, the total effective exposure time for the transfer streak is 2146 frames × 611 rows/frame ×41 μs/row = 53.7594 seconds.

It is important to note that this is the exposure time for the *source* counts. The background flux (measured using boxes parallel but above and below the source boxes) is caused by scattered photons from GX5-1, cosmic rays, and other sources. These events could arrive during the transfer streak, but are much more likely to occur during the 3.2 s hold time, so the appropriate exposure time is the full 6868.7 seconds. This is an unusual situation: the exposure times for the source and background photons in the source spectrum are different, and none of the standard spectral tools (XSPEC or Sherpa) can explicitly deal with it. We dealt with this problem by treating both the source and background as having the full exposure time of 6868.7 seconds, and then scaling the source flux by the ratio of the exposure times, 6868.7/53.7495 = 127.767.

After extracting the source and background spectra, we found an adequate fit using an absorbed bremsstrahlung model ($\chi^2_\nu = 1.2$) with $N_{\rm H} = 4.03 \pm 0.04 \times 10^{22}\,{\rm cm}^{-2}$, $kT = 10.5 \pm 0.5\,{\rm keV}$, and F_X(1-10 keV)$= 5.2 \times 10^{-8}\,{\rm erg/cm^2/s}$ (absorption corrected). Fortuitously, there was also a 9 ksec HETG observation of GX5-1 (Obsid 716) done July 18, 2000, only 19 days before the ACIS observation described here. Although GX5-1 is a variable source, the XTE All-Sky monitor shows little change between the two observations. In the 1.3-3.0 keV channel, the RXTE count rate was 14.2 ± 1.05 during the HETG observation and 13.4 ± 1.01 during our ACIS observation. In the 5.0-12.1 keV channel, the count rates were 32.3 ± 1.3 and 35.1 ± 1.3, respectively.

The HETG observations of GX5-1 have been analyzed by Ueda et al. (2005) in order to measure the elemental absorption along the line of sight. As noted in §1, they found the total $N_{\rm H} = 2.8^{+3.3}_{-1.8} \times 10^{22}\,{\rm cm}^{-2}$, based on extrapolation primarily from Mg, Si, S, and Fe absorption features. Their spectral model was more complicated than ours, but their total (absorption corrected) F_X(1-10 keV)$= 4.3 \times 10^{-8}\,{\rm erg/cm^2/s}$. This is $\sim$ 20% lower than our result from the transfer streak which may be due to true variation in the source. However, given the limited data available for the ACIS transfer streak, this 20% variation may also be due to calibration uncertainties. In any event, although this overall flux uncertainty will be reflected in the measured dust column density, but does not affect the profile of the halo.

3.3. Imaging Analysis

To calculate the radial profile of GX5-1, we first identified the serendipitous sources from the image, using the CIAO routine `celldetect`. We then selected an energy grid (1-4 keV, $\Delta E = 0.2\,{\rm keV}$) and a radial grid (100 points from 10-800", log-spaced). We filtered the data using the measured CCD energy, and extracted the counts in the radial profile using concentric annuli centered on the source. After making exposure maps for each energy band, we filtered out the regions with serendipitous sources in both the data and each exposure map. We then extracted the effective "radial exposure" using the same concentric annuli, for each energy band. Dividing the radial profile of the counts in each band by the effective area and exposure time gave the corrected radial profile in units of photons ${\rm cm}^{-2}\ {\rm s}^{-1}\ {\rm arcmin}^{-2}$ per energy band. We then divided this by the observed source flux in each band to get the fractional radial profile in units of source fraction ${\rm arcmin}^{-2}$. We fit this as the sum of the scattered halo, the *Chandra* PSF, and the background (both instrumental and cosmic). As with SES02, the *Chandra* PSF was measured from observations of Her X-1. We also note that the *Chandra* PSF is small enough that we can neglect scattering of the X-ray halo by the

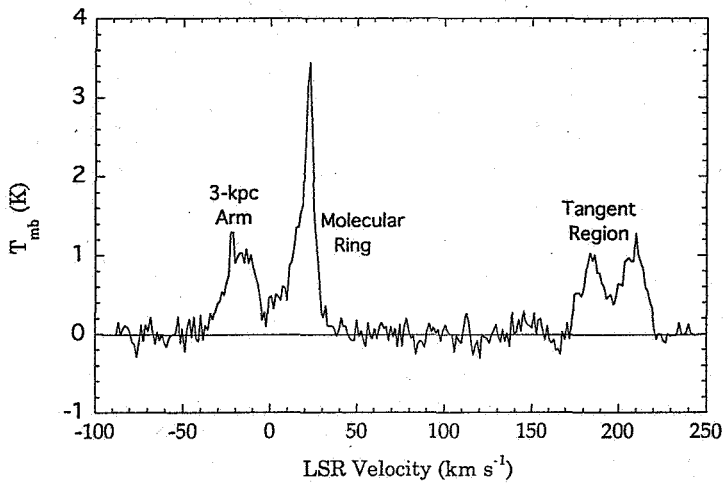

Fig. 3.— The CO emission observed in the direction of GX5-1 (Dame, Hartmann & Thaddeus 2001).

telescope. Finally, although the cosmic background is vignetted while the instrumental background is not, we found that in these bandpasses we could simply fit them together as a flat continuum out to 800″.

3.4. CO and 21 cm observations

The CO emission toward GX5-1 (Figure 3) is confined to 4 broad lines that can be readily associated with three distinct regions of the Galaxy. First, the line peaking near -22 km s^{-1} almost certainly arises from the 3 kpc Expanding Arm (e.g. Bania 1980), one of the best-defined spiral arms in the Galaxy. It is seen tangentially at $l \sim 24°$, implying a Galactic radius of 3.46 kpc. Since the inclination of the arm is unknown, we assumed it is circular to calculate its distance as 5.1 kpc at 5° longitude. A second region is associated with the line at 22 km s^{-1}, which arises from the so-called molecular ring. This is the region of high molecular cloud density roughly half-way between the Sun and the Galactic center. The near and far kinematic distances of this gas are 4.7 kpc and 12.1 kpc, with uncertainties of ±0.5 kpc imposed by the cloud-cloud velocity dispersion. At the far distance the molecular gas would lie 215 pc above the plane, more than 4 times the vertical dispersion of molecular clouds (Bronfman et al. 1988), so the near distance is far more likely.

Table 1: Cloud Positions from CO observations

Cloud	Velocity (km/s)	W_{CO} (K km/s)	$2\times N(H_2)$ (10^{20} cm^2)	N(HI) (10^{20} cm^2)	Position (kpc)
3 kpc Arm	-22	24.4	88 (or 18†)	34	5.1
Molecular Ring	22	40.4	146	34	4.7 (or 3.3)
Galactic center (Tangent) region	184, 208	21.7	16†	11	8.5
total		86.5	250	83	

†We have reduced the expected H_2 by a factor of 5, since molecular gas near the Galactic Center is thought to be anomalously bright in CO(e.g. Sodroski et al. 1995).

It is worth noting that most of the molecular ring emission closer to the plane at $l \sim 5°$ is centered roughly 10 km s^{-1} lower than that toward GX5-1; this (mildly) suggests that the molecular-ring emission toward GX5-1 might be anomalously high by that amount. If so, its kinematic distance should be reduced to ~ 3.3 kpc; this possibility is also noted in Table 1. We conclude that the molecular ring gas probably lies 3-5 kpc from the Sun. Given the extreme velocity crowding at this low longitude, it's possible that numerous clouds are spread over this range. A third region is associated with the other two partially-blended lines. These lines are at such high velocities ($\sim$ 200 km s^{-1}) that the emitting region must lie near the tangent point, at a Galactic radius of 0.7 kpc and thus near the Galactic center at a distance of ~ 8.5 kpc. Distances for the main molecular concentrations along the line of sight to GX5-1 are summarized in Table 1.

The molecular column density, $N(H_2)$, corresponding to each of the CO lines can be calculated from their velocity-integrated intensities, W_{CO}. For the molecular ring emission we use a standard Galactic value for $X \equiv N(H_2)/W_{CO} = 1.8 \times 10^{20}\,cm^{-2}K^{-1}km^{-1}s$ (Dame, Hartmann & Thaddeus 2001). Since there is evidence from both diffuse gamma ray emission (Blitz et al. 1985) and far infrared dust emission (Sodroski et al. 1995) that molecular clouds in the Galactic center region are anomalously bright in CO, we reduced X by a factor of 5 for the two high-velocity lines near the Galactic center. The molecular cloud in the 3 kpc Arm might also be anomalously bright in CO, given the arm's proximity to the Galactic center and large non-circular motion, but here for simplicity we apply the standard X. Our results are given in Table 1, along with the corresponding atomic column densities derived from the 21 cm survey of Hartmann & Burton (1997). The interpolated 21 cm spectrum toward the source shows velocity components similar to those seen in CO. We derived a total H I column density along the line of sight of $0.83 \times 10^{22}\,cm^{-2}$, in good agreement with the Dickey & Lockman (1990) value of $0.91 \times 10^{22}\,cm^{-2}$. The total gas column density, $2\times N(H_2) + N(H\,I)$, is calculated to be $3.1 \times 10^{22}\,cm^{-2}$.

As with many X-ray binaries, the true distance to GX5-1 is not well determined. We use the Christian & Swank (1997) upper limit of 9 kpc, based on its flux and calculated Eddington luminosity. Comparing this upper limit with Table 1 shows that GX5-1 is almost certainly behind the 3 kpc arm and the molecular ring, but may be in front of, behind, or embedded in the Galactic center region. The radial profile of the X-ray halo depends on the dust position relative to the source flux, but since X-ray halos are due to forward scattering, dust behind the source is unimportant.

4. Results and Discussion

GX5-1 is one of the brightest persistent X-ray sources in the Galaxy, and its relatively large absorption column density means that it has a substantial X-ray halo. The CO and H I observations also constrain the fit parameters. As a result, GX5-1 is one of the best sources to use in testing IS dust models. We therefore collected a wide range of proposed dust models: MRN77, Weingartner & Draine (2001, WD01), and the 15 models proposed in Zubko, Dwek & Arendt (2004, ZDA04) (most notably their BARE-GR-B model), as well as the model including extremely large grains discussed in Witt, Smith & Dwek (2001, WSD01). These models were developed to match optical, UV, and IR observations of dust primarily found in diffuse clouds (or, in the case of WSD01, *in-situ* data) without consideration of their X-ray scattering properties. Figure 4[Left] shows the size distributions for three of the these models, while Figure 4[Right] shows the distributions weighted by total cross section following Equation 1 (after integrating over all scattering angles; see Mathis & Lee (1991)). This shows that the differences in the largest grains must dominate the results. By systematically comparing all of these to the GX5-1 data, we can determine which models agree with the observed X-ray scattering, and which do not. However, it is important to realize that the dust grains

scattering the X-rays from GX5-1 are primarily in dense clouds, and may have quite different properties from the dust in diffuse clouds. Therefore, this study cannot globally exclude dust models, but simply determine which could describe the dust in dense clouds and which cannot.

Our results are additionally limited by the extreme pile-up, which obscures the true profile when $\theta < 100''$. Dust very near the source (*e.g.* the clouds in the Galactic center region) will lead to scattered photons in our insensitive "near region" (see also Figure 10) In addition, the number of scattered photons at every angle is proportional to $F_X N_H$, so errors in the measured flux linearly correlate with errors in the dust column density. Finally, the total column density towards the source is not well-known. The measurement by Christian & Swank (1997) of $N_{\rm H} = 2.54 \pm 0.19 \times 10^{22}\,{\rm cm}^{-2}$ is reasonably precise, but its accuracy depends entirely on the spectral model assumed. The Ueda et al. (2005) result of $N_{\rm H} = 2.8^{+3.3}_{-1.8} \times 10^{22}\,{\rm cm}^{-2}$, based on absorption features seen in high-resolution spectra, is accurate but far less precise. Considering the uncertainties on the HI large-scale optical depth the CO-to-H_2 conversion factor, the value of $N_{\rm H} = 3.9 \times 10^{22}\,{\rm cm}^{-2}$ derived from the gas tracers is probably only good to within a factor of 2. Based on all these results, the most we can say with confidence is that $N_{\rm H}$ is in the range $2 - 4 \times 10^{22}\,{\rm cm}^{-2}$. If our X-ray halo results are outside this range, it would imply is that the dust/gas mass ratio along this line of sight is abnormally high or low. Therefore, we cannot impart too much significance to the overall normalization of our results. However, we can require that the best-fit column density be independent of energy, and that the shape of the profile conform to the observations.

4.1. Smoothly Distributed Dust

Although the CO data strongly implies the dust along the line of sight is clumped, we begin with the simplest X-ray halo model, where the dust is assumed to be smoothly distributed along the line of sight ($f(x) \equiv 1$), and that it scatters the X-rays at most once (Predehl & Schmitt 1995). We begin by showing the radial profiles fit with some of the most common or best-fitting dust models, to show the quality of the results. Figure 5 shows the radial profile of GX5-1 at 1.5 ± 0.1 and $2.5 \pm 0.1\,{\rm keV}$, fit using a single-scattering smooth dust distribution. We show three different dust models: the classic MRN77 model as well as the more recent WD01 (with $R_V = 3.1, b_C = 6 \times 10^5$) and the BARE-GR-B model from ZDA04. The best-fit column densities were (respectively) 2.9, 2.1, and $4.2 \times 10^{22}\,{\rm cm}^{-2}$ at 1.5 keV and 2.7, 2.2, and $3.5 \times 10^{22}\,{\rm cm}^{-2}$ at 2.5 keV. At 1.5 keV all the fits were inadequate, although the ZDA04 model was the best fit. Although at 1.5 keV Mie effects could affect the halo slightly, a fit including these did not significantly change the results. However, as noted in §2.1, comparing with Figure 1 shows that including multiple scattering might have improved the ZDA04 model fit. Unfortunately, including multiple scattering from smoothly distributed dust in these fits is not yet possible. However, in the case of GX5-1 the dust is almost certainly *not* smoothly distributed and so this enhancement is left to a future paper. At 2.5 keV, Figure 1[Right] showed that multiple scattering is far less important, and we see in Figure 5[Right] that the ZDA04 model fit the radial profile of GX5-1 reasonably well– $\chi^2_\nu({\rm ZDA04}) = 1.8$. The MRN77 and WD01 models were still poor fits with $\chi^2_\nu({\rm MRN77}) = 9.4$ and $\chi^2_\nu({\rm WD01}) = 30$. They both overestimated the scattering at small angles and underestimated it at large angles far more than the ZDA04 model.

We then fit the GX5-1 radial profile data for energies between 2.5-3.5 keV (in 0.2 keV wide bins) to a model consisting of the *Chandra* PSF, a flat background, and the scattered halo calculated for smoothly-distributed dust following each of the above dust models. In Figure 6 we show the χ^2_ν values for each best-fit model. While none of the models are formally acceptable, clearly some are preferred. For example, none of the composite models of ZDA04 (those beginning with COMP-), with the possible exception of COMP-GR-

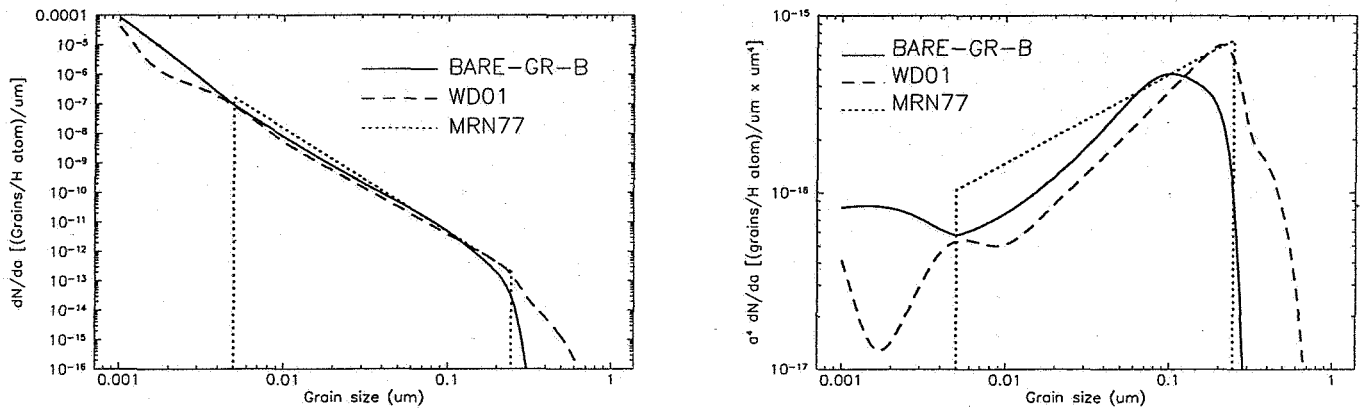

Fig. 4.— [Left] Total dust grain size distributions (summed over all components) for the ZDA04 BARE-GR-B model (solid line), the WD01 $R_V = 3.1$ model (dashed line), and the MRN77 model (dotted line). [Right] Same, but weighted by the RG X-ray total scattering cross section factor a^4.

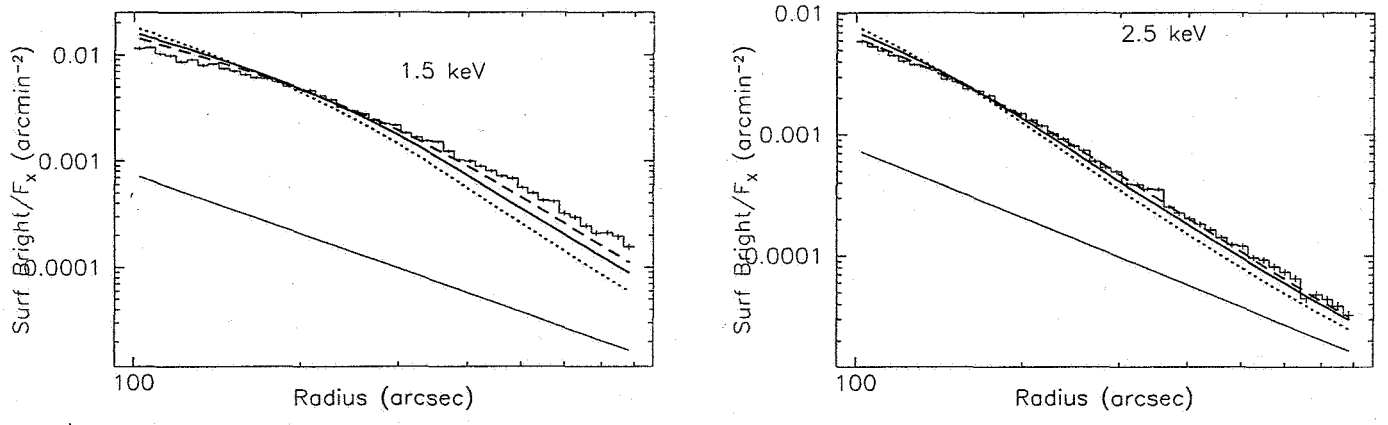

Fig. 5.— [Left] Fractional halo profile of GX5-1 at 1.5 keV, fit with a (single-scattering) smooth distribution using the MRN77 (solid line), WD01 (dotted line), and ZDA04 (dashed line) dust models. Multiple scattering is not included; including it would increase the model scattering at large angles and decrease it at small angles. The power-law fit to the *Chandra* PSF is also shown as a solid line.[Right] Same, at 2.5 keV, except that multiple scattering is much less significant.

B, are even close to a reduced $\chi^2_\nu \sim 1$, while the BARE-GR-B model is a reasonably good fit ($\chi^2_\nu = 1.5$), as would be expected from the results in Figure 5.

While instructive, Figure 6 is not conclusive. First, GX5-1's brightness means that the errors are probably not statistical but are instead dominated by calibration errors in the PSF and effective area. Second, the assumption of smoothly distributed dust disagrees strongly with the CO observations and is almost certainly incorrect. At the same time, the consistently poor fits found when using the composite models of ZDA04 suggests that these models poorly describe the observations. In Figure 7[Left] we show the fits to the radial profiles using the COMP-GR-B, COMP-AC-S, and COMP-NC-FG models. All of these over-predict the scattering at small angles and under-predict it at large angles. Since larger grains create smaller halos, this suggests that these models have relatively too many large grains. Interestingly, however, the best-fit column densities (shown in Figure 7[Right]) are almost all in the $2 - 4 \times 10^{22}\,\mathrm{cm}^{-2}$ range, with the exception of the last six models. In general, then, these models have problems not with the total mass of dust required, but rather the relative distribution of large and small grains.

4.2. Clumpy Cloud Models

Although the good smoothly-distributed ZDA04 BARE-GR-B model fit could be taken as evidence for that model over the others considered, we must also consider the possibility that the match is at least partially fortuitous as the dust is almost certainly clumped into the same cloud seen in CO emission. In this case the halo profile depends upon the relative positions of the clouds and the source. We start by considering the simplest possible model, a single cloud with variable relative position and column density. The parameters were allowed to vary freely without any assumptions taken from the CO observations. This model again includes only single scattering, since the cloud is treated as a single plane and there is no opportunity for multiple scattering. We begin with fits to the same three dust models (see Figure 8), and again find the best results from the ZDA04 BARE-GR-B model. At 2.5 keV, all models appears to fit equally well but only the ZDA04 BARE-GR-B model has plausible fit parameters. The best-fit column density for the MRN77, WD01, and BARE-GR-B models were $1.7, 1.2, 2.5 \times 10^{22}\,\mathrm{cm}^{-2}$, respectively and the best-fit dust position was $0.16, 0$, and 0.32. In both cases, the MRN77 and WD01 parameters are well outside the expected values. In addition, the BARE-GR-B model's best-fit column density appeared to be nearly constant with energy, unlike the other two models, and it had the lowest overall χ^2_ν values. The best-fit ZDA04 BARE-GR-B model had $N_{\rm H} = 2.5 \times 10^{22}\,\mathrm{cm}^{-2}$ and position $\sim 30\%$ of the distance to GX5-1, with slight variation between $25 - 35\%$ as a function of energy. Nonetheless, even this fit is formally unacceptable ($\chi^2_\nu > 2$) at most energies. Note that all fits strongly rejected the result found by Xiang, Zhang, & Yao (2005), who found $> 90\%$ of the dust to be very near the source.

We now consider a more complex spatial distribution of dust clouds, based on the CO data. The single cloud results foreshadow possible consistency problems between the scattered X-rays and a "naive" interpretation of the CO data. Even if the majority of the scattering is from the dust in the molecular ring, and it is in fact at 3.3 kpc rather than the expected value of 4.7 kpc, these results imply a large (if not impossible) distance for GX5-1 of $\sim 10\,\mathrm{kpc}$. We use a distance of 3.3 kpc for the molecular ring dust, and the lower dust column for the 3 kpc arm, after finding that the original values lead to a poorer fit to the data for all dust models. Of course, this may be an indication that there is a problem either in the calibration or the dust models, but we first examine if the closer distance can lead to a good result.

In Figure 9[Left] we used the results from the CO observations (see Table 1) to fix the cloud column

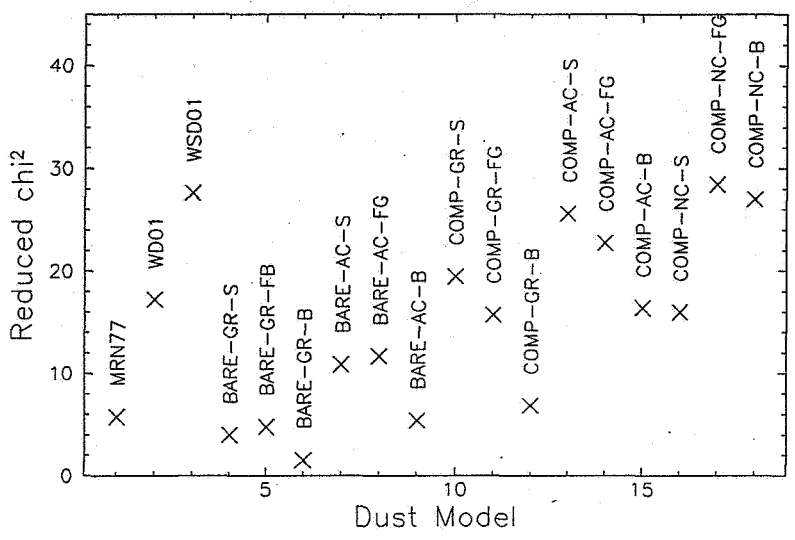

Fig. 6.— χ^2_ν values for each dust model used, assuming smoothly-distributed dust along the line of sight and using the data between 2.5-3.5 keV in 0.2 keV bins. At these energies, multiple scattering should be largely insignificant.

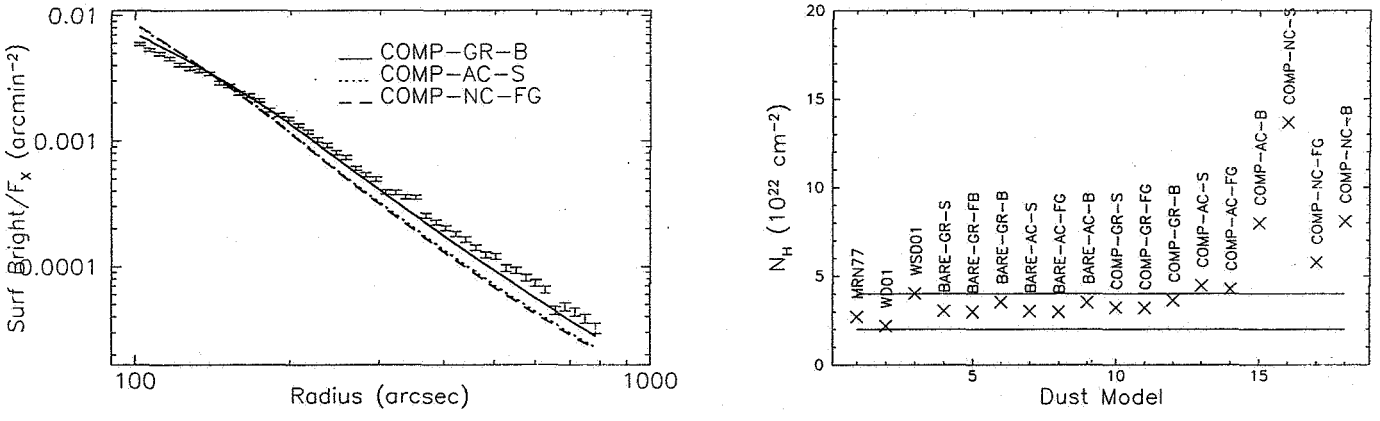

Fig. 7.— [Left] Radial profile of GX5-1 at 2.5 keV, with the best-fit ZDA04 COMP-GR-B, COMP-AC-S, and COMP-NC-FG models assuming smoothly-distributed dust. At large scattering angles these models all under-predict the total scattering, while at smaller angles ($< 150''$) the models overestimate the observed halo. [Right] The best-fit column density N_H for each model; the horizontal lines mark the expected upper and lower values. Most models find a reasonable total dust model, despite an overall poor fit.

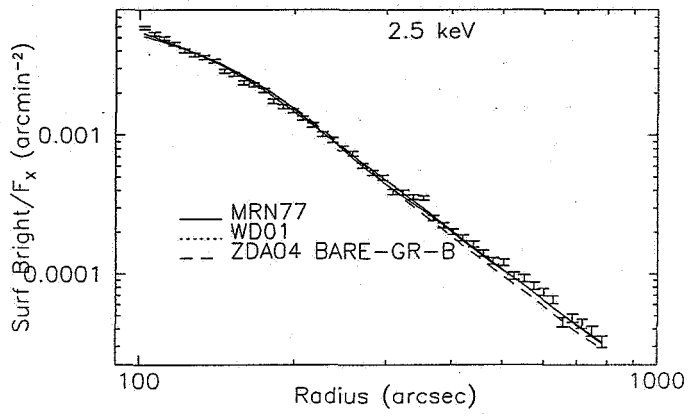

Fig. 8.— Best-fit scattered X-ray halo to the GX5-1 data for a single cloud at 2.5 keV. With the ZDA04 BARE-GR-B model, $N_{\rm H} = 2.5 \times 10^{22}$ and the cloud position is 33% of the distance to the source; $\chi^2_\nu = 2.1$. The MRN77 and WD01 models, despite their similar appearance, are worse fits with $\chi^2_\nu = 3.7, 5.7$ respectively.

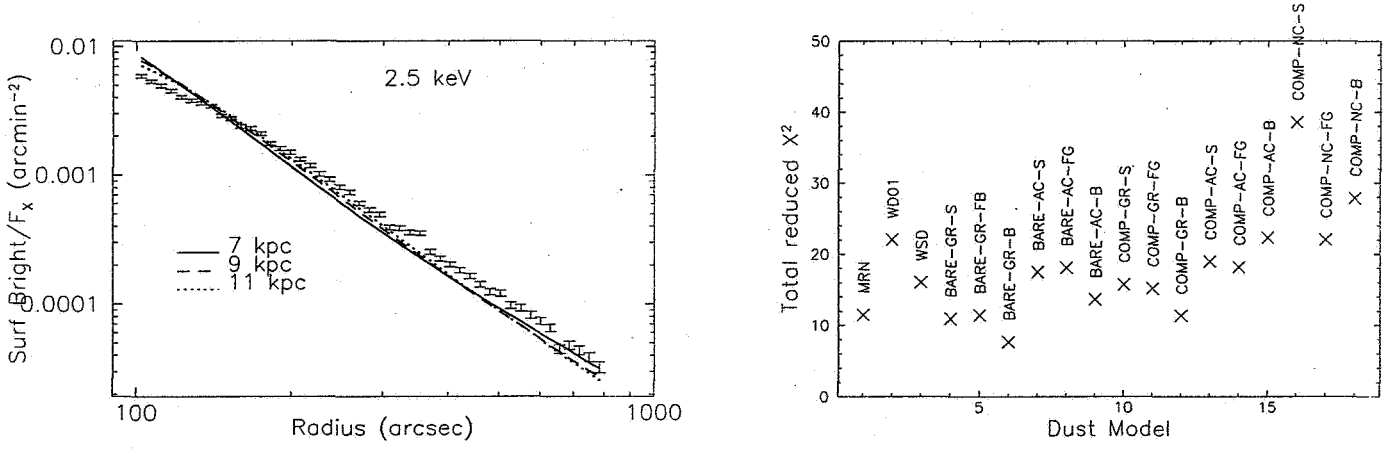

Fig. 9.— [Left] Observed radial profile (divided by source flux) at 2.5 keV with ZDA04 BARE-GR-B dust model using column densities and positions derived from the most plausible interpretation of the CO data with 3 possible source positions. [Right] χ^2_ν values for fits to the data between 2.5-3.5 keV (in 0.2 keV bins) for each dust model, assuming the same parameters and a source distance of 8 kpc.

densities and positions, and show the expected halos from a ZDA04 model considering single scattering only with three different positions. Again, the ZDA04 model fits were superior to either the MRN77 or WD01 models. A distance of 15 kpc is clearly a poor fit. The best-fit appears to be bracketed between the 7-9 kpc distances, although neither of these is an acceptable fit. In particular the predicted scattering is systematically high at 2.5 keV for a distance of 15 kpc. Only single-scattering was considered for these plots; multiple scattering would tend to broaden the halo slightly and might improve the fit slightly for the 7 and 9 kpc distances. However, as shown in Figure 1[Right], the improvement would only be marginal and is unlikely to explain the entire difference.

In Figure 9[Right] we again show the χ^2_ν values for each best-fit model, this time for the multiple cloud model as suggested by the CO data and assuming a distance for GX5-1 of 8 kpc, which most gave the best overall results. As with Figure 6, none of the models are formally acceptable, although some of the same models are again preferred, most notably the ZDA04 BARE-GR-B model. As with the smoothly-distributed dust model, the composite dust models of ZDA04, especially the "COMP-NC" models which use No Carbon, give very poor fits.

5. Conclusions

We have extracted the spectrum and scattered halo from GX5-1, one of the brightest Galactic X-ray binaries. Although the spectrum had to be extracted from the poorly-calibrated transfer streak, we were able to confirm the result due to a fortuitous HETG observation taken nearly contemporaneously with the ACIS observation along with the RXTE All-sky Monitor data. GX5-1 is so bright that pileup was evident out to a radius of 100″. Nonetheless, we were able to extract reliable surface brightness profiles between $100 - 800''$. GX5-1 has a large (but rather poorly determined) column density which is likely in the range $2 - 4 \times 10^{22}\,\mathrm{cm}^{-2}$. It is also close enough to the Galactic plane that velocity-resolved CO measurements exist which show the presence of a number of dense clouds along the line of sight.

We have shown that GX5-1's column density is large enough that X-rays with energies below 2 keV are often scattered multiple times by dust along the line of sight. Since this is a complication to fitting, we limited our fitting to energies above 2.5 keV where multiple scattering is much less significant. We compared our observations to a wide range of dust grain models, including for the first time the many models described in ZDA04. We found reasonable fits for some dust models assuming either a smooth dust distribution or a single "cloud" along the line of sight. No dust grain model fit the default parameters determined from the CO data for any distance to GX5-1. However, the fit parameters found when using a single cloud suggested a re-examination of the CO data. The 3 kpc Arm (at 5.1 kpc) is on the boundary between the Galactic center, where the CO is anomalously bright (Sodroski et al. 1995), and the Galactic disk. If the gas in the 3 kpc Arm is in fact similar to the Galactic center emission, it would have only 1/5th of the gas (and thus dust) than predicted in Table 1. In this case, the dominant dust cloud would be the one in the Molecular Ring, which at 3.3 kpc is roughly 1/3 of the distance to the Galactic center and which has a predicted hydrogen column density of $\sim 1.8 \times 10^{22}\,\mathrm{cm}^{-2}$. Our best-fit single cloud model had $N_\mathrm{H} = 2.5 \times 10^{22}\,\mathrm{cm}^{-2}$ at about this distance, in reasonbly good agreement. More data from X-ray binaries at or near the Galactic center are needed to see if in fact these results hold for other X-ray halo observations in this area, or are merely special pleading.

We also note our strong disagreement with the results of Xiang, Zhang, & Yao (2005) regarding the dust density along the line of sight. Although we are not as sensitive to dust near the source as their observation,

the effects would still be noticeable in our results. We do not know the origin of this discrepancy, but note that they found significant amounts of dust near all of their sources. It seems possible that there may be calibration issues, especially in the zero-order of the HETG, which are in some part responsible for their result.

We also found that some dust grain models strongly disagreed with the observations in all cases. Most notably, nearly all of the Composite dust models of ZDA04 (models beginning with COMP-) disagreed strongly with the data (the sole exception is the COMP-GR-B model). The composite "No Carbon" (COMP-NC) models in particular were uniformly poor descriptions. The BARE-GR-B model, which combines bare graphite and silicate grains with PAHs using B star abundances, was the overall best fitting model in all cases. However, since no dust model or spatial distribution led to $\chi^2_\nu \sim 1$ fits, and given remaining uncertainties in the calibration and the modeling we can not state that this dust model is "preferred."

The idea of directly measuring the IS dust mass, composition, and size distribution is enticing enough that it appears in every proposal to observe X-ray halos. However the history of astronomical X-ray scattering halo results shows that there are difficulties arising from the many assumptions needed before the data can be modeled. Although not conclusive, our results show that adding CO and HI observations do help in reducing the allowed model space and putting better constraints on the dust models. However, the uncertainties in the CO and HI analysis must be included to sensibly use this additional data. We plan to test our results by analyzing more Galactic Center sources to see if, for example, they also imply that the 3 kpc Arm is CO-bright. Another way to break the existing near-degeneracy between dust models would be to obtain measurements of the radial profile between $10''-100''$. Figure 10 shows that variations in dust grain positions affect the surface brightness at these angular distances far more than in the $100-800''$ region measurable with our data. We have just obtained *Chandra* HRC-I observations of GX5-1 which will measure the radial profile in this range (albeit without energy resolution).

REFERENCES

Bandyopadhyay, R. M., Shahbaz, T., & Charles, P. A. 2003, MNRAS, 340, L13

Bania, T. M. 1980, ApJ, 242, 95

Berendsen, S. G. H., Fender, R, Kuulkers, E., Heise, J. & van der Klis, M. 2000, MNRAS, 318, 599

Blitz, L., Bloemen, J. B. G. M., Hermsen, W. & Bania, T. M. 1985, A&A, 143, 267

Bronfman, L., Cohen, R. S., Alvarez, H., May, J. & Thaddeus, P. 1988, ApJ, 324, 248

Christian, D. J. & Swank, J. H. 1997, ApJSS, 109, 177

Dame, T. M., Hartmann, D. & Thaddeus, P. 2001, ApJ, 547, 792

Davis, J. E. 2001, ApJ, 562, 575

Dickey & Lockman, J. 1990, ARA&A, 28, 21

Draine, B. T., & Lee, H. M. 1984, ApJ, 285, 89

Draine, B. T. 2003, ApJ, 598, 1026

Guinier, A. & Fournet, G. 1955, *Small-angle Scattering of X-rays* (New York: Wiley)

Hartmann, D. & Burton, W. B. 1997, Cambridge; New York: Cambridge University Press

Henke, B. L. 1981, in "Low Energy X-Ray Diagnostics", ed. D. T. Attwood and B. L. Henke (New York, AIP)

Jonker, P. G., Fender, R.P., Hambly, N. C. & van der Klis, M. 2000, MNRAS, 315, L57

van der Klis, M., 1995 in Lewin W.H.G, van Paradijs, J, and van den Heuvel E.P.J., eds., X-ray Binaries (Chapter 6), Cambridge University Press, p. 252

Mathis, J. S., Rumpl, W. & Nordsieck, K. H. 1977, ApJ, 280, 425 (MRN77)

Mathis, J. S. & Lee, C. W. 1991, ApJ, 376, 490

Mauche, C. W. & Gorenstein, P. 1986, ApJ, 302, 371

Overbeck, J. W. 1965, ApJ, 141, 864

Predehl, P., Schmitt, J., Snowden, S. & Trümper, J. 1992, Science, 257, 935

Predehl, P. & Schmitt, J. 1995, A&A, 293, 889

Predehl, P. & Klose, S. 1996, A&A, 306, 283

Smith, R. K. & Dwek, E. 1998, ApJ, 503, 831

Smith, R. K., Edgar, R. J. & Shafer, R. A. 2002, ApJ, 581, 562 (SES02)

Sodroski, T. J., et al. 1995, ApJ, 452, 262

Ueda, Y., Mitsuda, K, Murakami, H., & Matsushita, K. 2005, ApJ, 620, 274

Weingartner, J. & Draine, B. 2001, ApJ, 548, 296 (WD01)

Witt, A. N., Smith, R. K., & Dwek, E. 2001, ApJL, 550, L201

Xiang, J., Zhang, S. N. & Yao, Y. 2005, astro-ph/0503256

Zubko, V., Dwek, E. & Arendt, R. 2004, ApJS, 152, 211 (ZDA04)

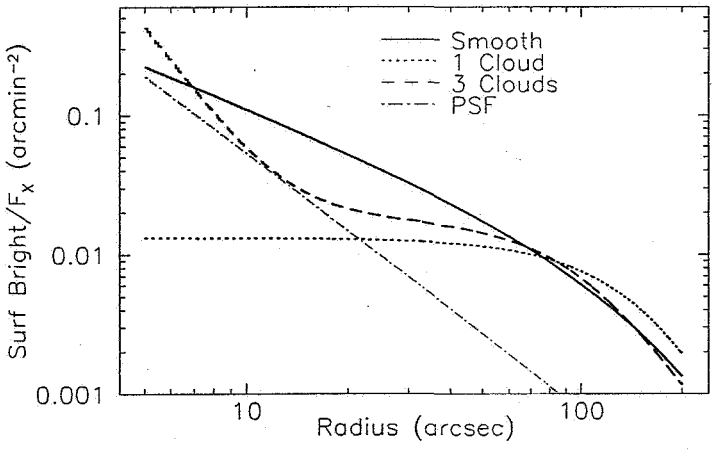

Fig. 10.— Predicted near-source X-ray halos at 2.5 keV using the ZDA04 BARE-GR-B model with total $N_{\rm H} = 3.91 \times 10^{22}\,{\rm cm}^{-2}$. Three different dust position distributions are shown: smoothly distributed dust, a single cloud 1/3 of the distance to GX5-1, and three clouds at the positions predicted by the CO data, assuming a source distance of 8.51 kpc.